Biochar/Zinc Oxide Composites as Effective Catalysts for Electrochemical CO2 Reduction

ACS Sustainable Chemistry & Engineering

pubs.acs.org/journal/ascecg

Research Article

Biochar/Zinc Oxide Composites as Effective Catalysts for Electrochemical CO_2 Reduction

Mirtha A. O. Lourenço,*,§ Juqin Zeng,*,§ Pravin Jagdale, Micaela Castellino, Adriano Sacco, M. Amin Farkhondehfal, and Candido F. Pirri

Cite This: *ACS Sustainable Chem. Eng.* 2021, 9, 5445−5453

Read Online

ACCESS | Metrics & More | Article Recommendations | Supporting Information

ABSTRACT: Novel electrocatalysts based on zinc oxide (ZnO) and biochars are prepared through a simple and scalable route and are proposed for the electrocatalytic reduction of CO_2 (CO_2RR). Materials with different weight ratios of ZnO to biochars, namely, pyrolyzed chitosan (CTO) and pyrolyzed brewed waste coffee (CBC), are synthesized and thoroughly characterized. The physicochemical properties of the materials are correlated with the CO_2RR to CO performance in a comprehensive study. Both the type and weight percentage of biochar significantly influence the catalytic performance of the composite. CTO, which has pyridinic- and pyridone-N species in its structure, outperforms CBC as a carbon matrix for ZnO particles, as evidenced by a higher CO selectivity and an enhanced current density at the ZnO_CTO electrode under the same conditions. The study on various ZnO to CTO weight ratios shows that the composite with 40.6 wt % of biochar shows the best performance, with the CO selectivity peaked at 85.8% at −1.1 V *versus* the reversible hydrogen electrode (RHE) and a CO partial current density of 75.6 mA cm^{-2} at −1.3 V *versus* RHE. It also demonstrates good stability during the long-term CO_2 electrolysis, showing high retention in both CO selectivity and electrode activity.

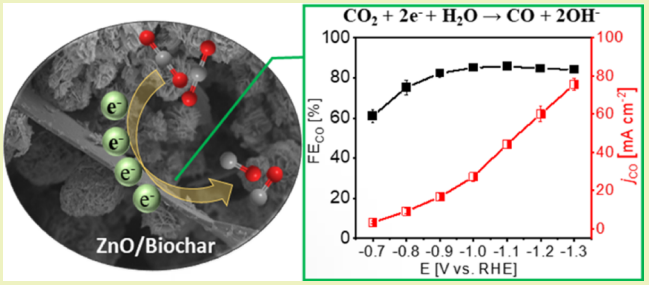

KEYWORDS: *carbon dioxide, zinc oxide, biochar, electrocatalysis, carbon monoxide*

INTRODUCTION

The electrochemical conversion of carbon dioxide (CO_2) to valuable fuels and chemicals using renewable electricity while reducing CO_2 emissions is of high economic and environmental interest.[1,2] Among many products from the electrochemical CO_2 reduction reaction (CO_2RR), carbon monoxide (CO) is considered the most important one as it has high relevance for the chemical industry.[3−6] It is a versatile C1-building block and is intensively used in large-scale industrial processes such as the Fischer−Tropsch synthesis of hydrocarbons[7] and Monsanto/Cativa acetic acid synthesis.[8] Despite the CO_2RR being an appealing technology, it presents some drawbacks associated with high kinetic barriers, multistep reactions, and competitive hydrogen evolution reaction (HER), leading to a high overpotential, a poor conversion rate, and low selectivity.[2] To overcome these issues, sustainable, cost-efficient, and high-performance electrocatalysts capable of efficiently converting CO_2 into CO must be developed.[9,10] For this purpose, different metal electrodes such as gold (Au),[11−13] silver (Ag),[14] palladium (Pd),[15] and zinc (Zn)[16−18] have been suggested. Among these metals, Zn is the most interesting one to be applied at a large scale for the CO_2RR to CO, as it is an inexpensive and abundant non-noble metal.[18] Monometallic Zn-based electrocatalysts can be obtained with different particle shapes and porosities, showing good performance for converting CO_2 to CO.[16−20] Zn metal can be combined with other metals, for example, copper (Cu),[21,22] to obtain enhanced efficacy and selectivity. However, Cu is a relatively expensive metal, and cheap alternatives to Cu are rarely exploited in the preparation of enhanced Zn-based catalysts for the same function. For instance, there is a scarcity of data about the incorporation of carbon sources to Zn materials to reduce the cost and to increase the efficiency of the electrocatalysts in the CO_2RR application. Just a few studies for the preparation of Zn−C-based materials were reported, but for supercapacitors[23,24] and photocatalysis[25,26] applications. In the case of the CO_2RR, some examples of the preparation of reduced graphene oxide (rGO)-based catalysts were described but using expensive sources such as Cu, Au, nickel (Ni), Ag, cobalt (Co)-porphyrin, and iron (Fe)-porphyrin materials.[27] Recently, Zn/rGO electrodes were prepared and tested in the CO_2RR, with a CO Faradaic efficiency of 85% at −0.84 V *versus* reversible

Received: February 5, 2021
Revised: March 18, 2021
Published: April 7, 2021

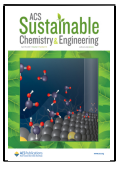

hydrogen electrode (RHE) in a CO_2-saturated 0.5 M $KHCO_3$ solution.[28] In general, the authors observed that the addition of rGO improved the distribution and conductivity of the catalysts.[27,28] However, most of the rGO-based electrocatalysts, described to date, have a low-operation durability, and the production at the industrial scale is environmentally and economically unviable.[27] The use of rGO as a carbon source is not sustainable as its synthesis is typically made by the oxidation of graphite using strong acids that are harmful to human safety and the environment.[29] Thus, greener carbon sources, capable of improving the dispersion and conductivity of the catalysts, should be combined with ZnO.

Remarkable advancement can be anticipated for the industry if sustainable and cost-efficient catalysts can be prepared from waste sources and can enable selective and long-term CO_2 electrolysis. Herein, we report a novel study on the preparation of biochar-ZnO composites and their electrocatalytic behavior in the CO_2RR, involving the materials' physical and chemical properties. To the best of our knowledge, two carbon sources, prevenient from the pyrolysis of brewing coffee and chitosan residues, were used for the first time to anchor ZnO particles through an *in situ* and low-temperature approach. The biochar/ZnO materials were applied in the CO_2RR, and their electrocatalytic performance was assessed and compared at two rationally chosen potentials, −0.89 and −1.09 V, *versus* the RHE in a batch reactor. Electrochemical impedance spectroscopy and CO_2 adsorption selectivity over N_2 experiments were performed to elucidate the synergetic effect between carbon and ZnO in the CO_2RR. The best-performing sample was also tested in a semiflow cell in a wide potential range.

MATERIALS AND METHODS

Materials Synthesis. *ZnO/Biochar Catalysts.* $Zn(NO_3)_2{\cdot}6H_2O$ (0.37 g) was dissolved in Milli-Q water (2.5 mL) and stirred for 1 h at 70 °C in a closed glass vial. In another vial, a varied amount of pyrolyzed chitosan (CTO) or brewed coffee (CBC; see biochar synthesis details in the Supporting Information) was dispersed in 1 M solution of NaOH (2.5 mL) through sonication for 10 min at 37 kHz. The zinc nitrate solution was added dropwise to the pyrolyzed biomass dispersion under vigorous stirring at room temperature. The mixture was stirred for 2 h. After centrifugation (at 4000 rpm and 5 min), the powders were washed thrice with double distilled water and then once with ethanol. The obtained gray powders were dried in an oven at 80 °C to get ZnO/CTO_*x* or ZnO/CBC_*x*, where *x* can be 1, 2, and 3 and corresponds to the pyrolyzed biomass weight percentage with respect to the zinc precursor (6.4, 21.0, and 35.4 wt %, respectively). For comparison reasons, a ZnO sample was also prepared using the same procedure but without adding the pyrolyzed biomass to the NaOH solution.

Characterization of the As-prepared Catalysts. The materials were characterized by thermogravimetric analysis (TGA), powder X-ray diffraction (XRD), scanning electron microscopy (SEM), Raman and Fourier transform infrared (FTIR) spectroscopies, and X-ray photoelectron spectroscopy (XPS). For selected samples, operando TGA−infrared (IR) spectroscopy was performed to study the adsorption of CO_2 from a CO_2/N_2 gas mixture. The equipment and experimental parameters used are described in the Supporting Information.

Electrochemical Characterization. Electrodes were prepared through coating carbon paper by the drop-casting method with a catalyst mass of ∼2.3 mg·cm^{-2}. Details are described in the Supporting Information.

Electrochemical impedance spectroscopy (EIS) measurements were performed in a three-electrode cell at room temperature with a CHI760D electrochemical workstation, as detailed in the Supporting Information.

Chronoamperometric (CA) measurements were carried out by using a CHI760D electrochemical workstation, and the products of the CO_2RR were analyzed contemporarily, as shown in the Supporting Information.

RESULTS AND DISCUSSION

Materials Characterization. The carbon weight percentage incorporated into ZnO-based samples was determined by TG analyses (see Figure S1 and Table S1 in the Supporting Information for a detailed description). As shown in Table S1, ZnO/CTO_*x* and ZnO/CBC_*x* (*x* = 1, 2, or 3) show comparable carbon percentages of 19.1 and 15.2% in ZnO/CTO_1 and ZnO/CBC_1, respectively, of 40.6 and 37.7% in ZnO/CTO_2 and ZnO/CBC_2, respectively, and of 50.9 and 46.5% in ZnO/CTO_3 and ZnO/CBC_3, respectively. For each ZnO/biochar family (ZnO/CTO or ZnO/CBC), the weight percentage of carbon introduced increased with the increase of biochar in the synthesis.

Figure 1 shows the XRD patterns of all ZnO-based materials. In the ZnO sample, crystalline ZnO presents a hexagonal

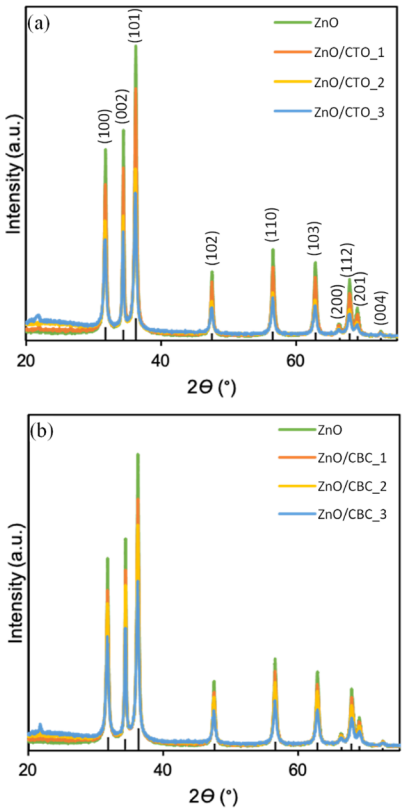

Figure 1. XRD patterns of (a) ZnO/CTO_*x* and (b) ZnO/CBC_*x* materials. Black bars refer to the wurtzite JCPDS reference card (36-1451).

wurtzite structure (JCPDS card file 36-1451) with a space group of *P*63*mc*. The diffraction peaks at 2θ = 31.8, 34.4, 36.2, 47.6, 56.6, 62.9, 66.8, 67.9, 69.1, and 72.7° correspond to the reflections from the (100), (002), (101), (102), (110), (103), (200), (112), (201), (004), and (202) planes, respectively.[30] The absence of additional peaks indicates the high purity of the prepared ZnO sample. All ZnO/biochar electrocatalysts display the diffraction peaks indexed to ZnO with the

https://doi.org/10.1021/acssuschemeng.1c00837
ACS Sustainable Chem. Eng. 2021, 9, 5445−5453

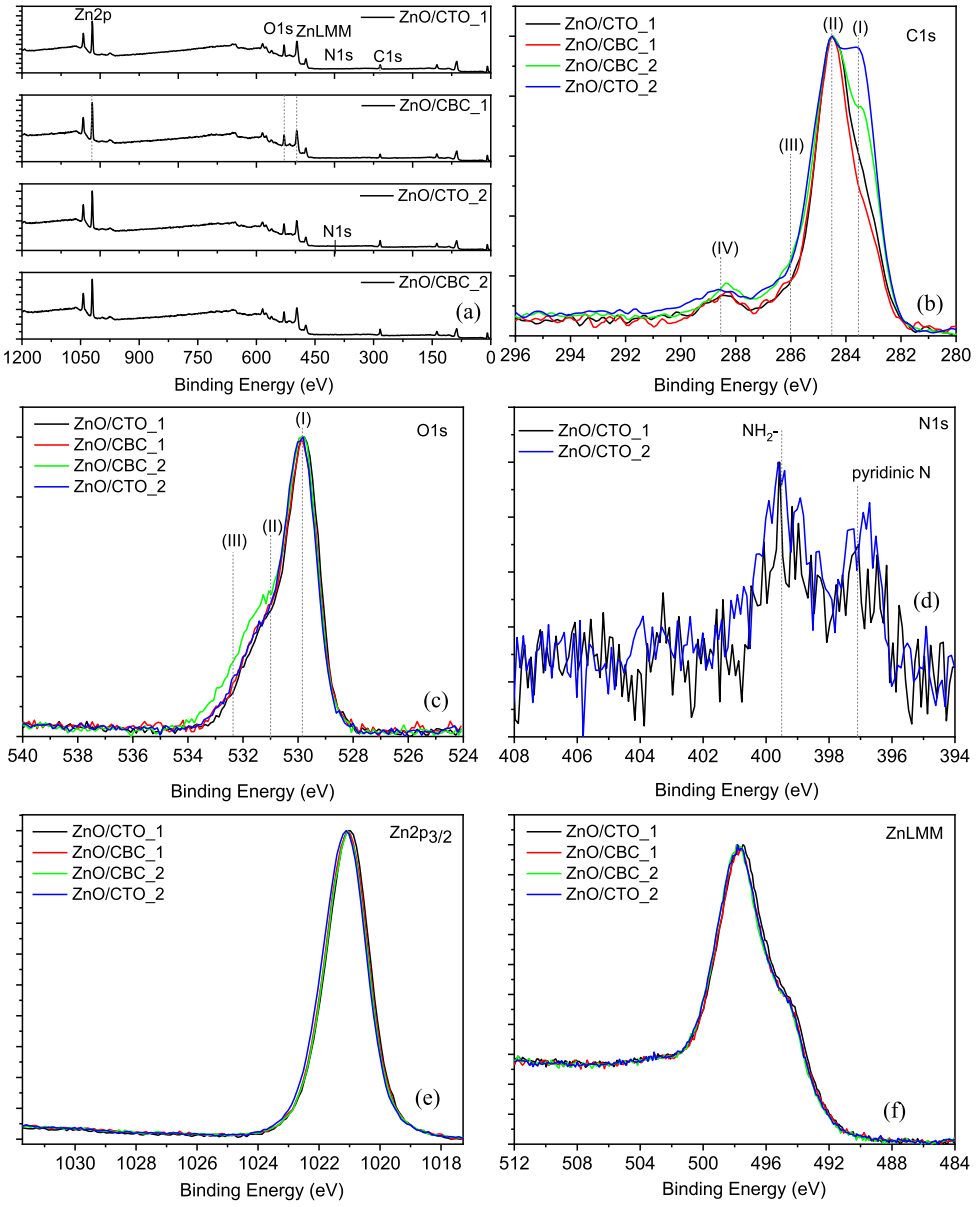

Figure 2. XPS survey (a) and normalized HR scans: C 1s (b), O 1s (c), N 1s (d), Zn $2p_{3/2}$ (e), and Auger ZnLMM (f) for four selected samples.

hexagonal wurtzite structure, and these peaks are intense and sharp, suggesting that the presence of carbon has no significant effect on the crystalline structure of ZnO. Diffraction peaks at 2θ = 24°−30° related to the crystalline graphitic layers of carbonaceous materials are absent[31] on both ZnO/CTO_*x* and ZnO/CBC_*x* materials (Figure S2), which can be related to the smaller content of carbonaceous species with respect to the pristine biochar materials.

The morphologies of the ZnO-based samples were studied by FESEM. The ZnO sample (Figure S3a) shows a three-dimensional (3D) flower-like architecture with about 2 μm in diameter, constituted of interleaving thin plates or nanosheets (between 11 and 16 nm of thickness, Figure S3b) that grow in a helical style.[32,33] Independent of the added CTO or CBC carbon amount on ZnO/CTO or ZnO/CBC samples, most ZnO maintains its microflower structure as well as the size of the plates or nanosheets (*cf.* Figure S3c−f). It is also observed that some of the microflowers and/or the nanosheets grew on CTO or CBC.

The FTIR and Raman spectra of ZnO and ZnO/biochar materials are illustrated in Figures S4 and S5. Raman data supported the presence of the hexagonal wurtzite phase of ZnO,[30] confirming the good crystallinity of ZnO in all samples, as observed by XRD. Moreover, both spectroscopies indicated a possible chemical bond between carbon and ZnO (further discussion in the Supporting Information).

XPS analysis has been performed to understand deeply the role of the chemical shifts due to the matrix and pyrolyzed biomass interface interaction (Figure 2). The survey spectra (Figure 2a) show the presence of Zn, O, and C in all the four samples analyzed (ZnO/CTO_1/2 and ZnO/CBC_1/2) and N only in the chitosan-containing ones. It is worth noticing that the increase of biochar percentage is clearly reflected in the increase in the relative amounts of C and N (Table S2, in the Supporting Information), as expected. From the deconvolution of the C 1s photoelectron peak (fitting curves not reported), four peaks are obtained (see Figure 2b and Table S3): peak I at 283.3 eV due to Zn−C or Zn−C

https://doi.org/10.1021/acssuschemeng.1c00837
ACS Sustainable Chem. Eng. 2021, 9, 5445−5453

connected with an oxygen vacancy (O_{vac}) bond, peak II at 284.5 eV due to C−C sp^2 hybridization, peak III at 286.2 eV due to C−O−Zn/N/O bonds, and peak IV at 288.5 eV due to −C═O/O−C−O.[34] The presence of peak I is fundamental in order to be able to confirm the direct bond between the ZnO structures and the biochar materials.[35] We can state that this new bond is related only to the presence of ZnO bonded to biochar materials because previous measurements made on the same carbonaceous precursors, that is, wasted coffee[36] and pyrolyzed chitosan,[37] have shown no signal related to this chemical shift. The relative intensity of this peak (see Figure 2 and Table S3) is directly correlated with the percentage of CBC and CTO. From the O 1s peak deconvolution (fitting curves not reported), three peaks have been assigned to the following chemical shifts (see Figure 2c and Table S3): peak I at 529.8 eV due to O−Zn, peak II at 531.3 eV due to O_{vac}[38] and OH/C═O groups, and peak III at 532.8 eV due to H_2O/C−O species. The four photoelectron curves are mostly perfectly overlapped apart from a slight increase in peak III for the ZnO/CBC_2 sample. For the CTO-containing samples, we have also analyzed the N1s peak (Figure 2d). From its fitting procedure, two well-separated peaks are obtained due to pyridinic-N (at 397.1 eV) and pyridone- or pyrrole-like N (at 399.5 eV).[39−41] As the CTO biochar was treated at 800 °C for 2 h, the presence of pyridone-N is more likely than that of pyrrole-like N, as the former is more stable at elevated temperatures.[42]

The analysis of the Zn $2p_{3/2}$ peak is shown in Figure 2e. According to the literature,[43,44] ZnO compounds show different chemical shifts due to the level of nano- or microstructuring of their surfaces (particles, flowers, rods, *etc.*). Hence, the Zn $2p_{3/2}$ position should be located in the range of 1020.7−1021.2 eV. Our samples show four almost perfectly overlapped peaks located between 1021.0 and 1021.2 eV. We further checked the ZnLMM Auger peak (Figure 2f) and calculated the modified Auger parameter. This constant value is powerful to discriminate among different oxidation states of some elements (such as Zn, Cu, Ni, *etc.*) in which the chemical shifts are not pronounced and evident in the photoelectron peaks, according to the possible bonds available.[45] The modified Auger parameter values for all the samples are in the range between 2010.0 and 2010.1 eV, which are assigned to ZnO.[46] Thus, XPS analysis confirms the presence of a direct link between the ZnO microstructures and the biochar materials.

CO_2 Electrolysis in a Batch Cell. In order to compare the activity and selectivity of various electrodes for the CO_2RR, CA measurements were carried out in a batch cell with online μGC analysis (Scheme S2a). According to the literature, a plain Zn electrode becomes selective for CO formation at about −0.9 V, and its selectivity for CO increases by negatively shifting the applied potentials, whereas nanostructured Zn-based electrodes commonly have the highest CO selectivity from −0.85 to −1.0 V.[18,20,47,48] Hence, two applied potentials, −0.89 and −1.09 V, are rationally chosen.

Figures S6−S14 show the *i*−*t* curves and product analyses of all electrodes at both potentials. At the ZnO-containing electrodes, the current density initially decreases due to the reduction of oxides in the electrode.[48] ZnO can reduce or partially reduce at negative potentials (<−0.5 V).[48] By the operando X-ray absorption fine-structure spectroscopy measurements, Jeon *et al.*[17] demonstrated the coexistence of cationic Zn species and metallic Zn during the CO_2RR. However, Rosen *et al.*[20] demonstrated that the nanostructured Zn-based catalyst is reduced to metallic Zn and is structurally stable at potentials more negative than −0.7 V through in situ/operando X-ray absorption spectroscopy measurements. Hence, the real oxidation state of Zn under the CO_2RR is still not clear, and more operando analyses are required, which are not the scope of this work. At each electrode, the reductive current density increases by negatively shifting the applied potential. The concentrations of gaseous products were determined by μGC every 3−4 min. No other gas-phase products beyond H_2 and CO were detected. The concentrations of liquid products in the catholyte were determined by HPLC at the end of each test. HCOOH is the only detected liquid product. All electrodes show a minor selectivity for the HCOOH formation as the FE_{HCOOH} values reach low values of 1.5−3.0% in the investigated potential range.

The selectivity and activity of various electrodes are compared in Figure 3. Both CTO and CBC electrodes have

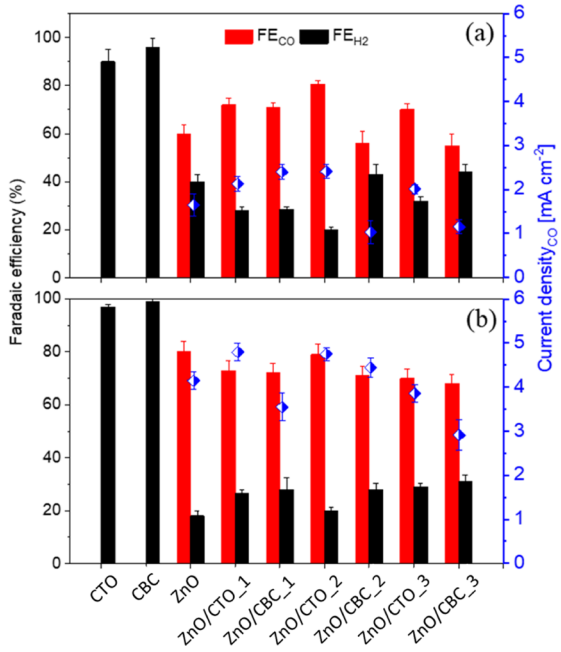

Figure 3. Faradaic efficiency values for CO and H_2 formation and partial current densities for CO production at various electrodes in 0.1 M $KHCO_3$ electrolyte at (a) −0.89 and (b) −1.09 V.

no selectivity for the CO_2RR as FE_{H_2} reaches more than 90% at both potentials and no CO is detected. The ZnO electrode has good selectivity for CO formation, with FE_{CO} of 60 and 80% at −0.89 and −1.09 V, respectively, in agreement with the reported results on ZnO-based catalysts.[19,20,49] As shown in Figure 3a, the selectivity for CO is enhanced by applying the ZnO/CTO catalyst at −0.89 V. The percentage of CTO can be increased to 50.9 wt % in the catalyst while maintaining good FE_{CO} (≥70%). Each ZnO/CBC_*x* (*x* = 1, 2, or 3) shows relatively lower FE_{CO} than ZnO/CTO_*x*. With respect to the ZnO electrode, the ZnO/CBC electrode with 15.2 wt % of CBC exhibits enhanced CO selectivity, whereas those with higher CBC contents show inferior FE_{CO} values. At a more negative potential of −1.09 V (Figure 3b), all ZnO/carbon electrodes achieve good selectivity for CO (FE_{CO} ≥ 70), independent of the carbon types and carbon percentages. At this potential, each ZnO/CTO_*x* (*x* = 1, 2, or 3) sample still

https://doi.org/10.1021/acssuschemeng.1c00837
ACS Sustainable Chem. Eng. 2021, 9, 5445−5453

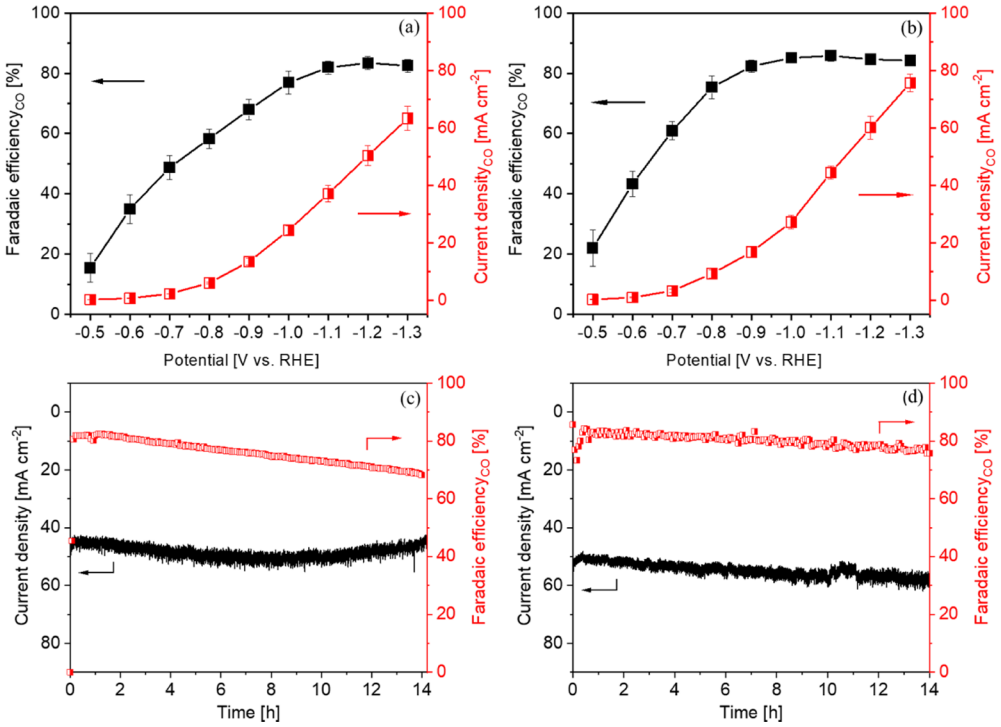

Figure 4. CO_2RR in a semiflow reactor in 2.0 M $KHCO_3$ electrolyte: FE_{CO} and CO partial current densities at various potentials on the (a) ZnO electrode and (b) ZnO/CTO_2 electrode; stability test at −1.1 V on the (c) ZnO electrode and (d) ZnO/CTO_2 electrode.

shows slightly higher FE_{CO} than ZnO/CBC_*x* with a similar carbon content. Among all the samples, the ZnO/CTO_2 electrode shows the best CO selectivity at both potentials.

Partial current density for CO formation can be obtained by multiplying FE_{CO} by the geometric current density (Figure S15). As shown in Figure 3, the ZnO/CTO electrodes show raised CO formation rates at relatively low CTO percentages (19.1 and 40.6 wt %) and maintain a similar CO production rate at a higher carbon content (50.9 wt %) compared to the ZnO electrode at each potential. In general, the ZnO/CBC electrode shows inferior performance compared to the ZnO/CTO one with a similar carbon content at each potential. By normalizing the partial current density by the mass loading of ZnO in the electrode, we obtained the mass activity of the electrode for the CO_2RR to CO and compared them in Figure S16. The addition of CTO support can significantly increase the mass activity of ZnO for the CO_2RR to CO. Particularly, the ZnO/CTO electrodes containing 40.6−50.9 wt % of CTO show comparable normalized current densities of 1.8 mA·mg_{ZnO}^{-1} at −0.89 V and 3.4 mA·mg_{ZnO}^{-1} at −1.09 V, remarkably higher than those obtained at the ZnO electrodes at the same potential and slightly enhanced with respect to our previous work.[48] In contrast, the CBC addition shows no consistent improvement in the mass activity.

Concisely, the CO_2RR on the ZnO/C electrodes is dependent on the type of the biochar and the applied potential. Comparing two kinds of biochar carbon matrices for ZnO, the CTO outperforms CBC in terms of both selectivity and activity for the CO_2RR. It is widely accepted that the pyridinic- and pyridone-N can create Lewis basic sites and interact with CO_2 molecules to enable facile CO_2 adsorption.[37,39,50−52] To understand the CO_2 adsorption behavior, the CO_2 selectivity over N_2 was measured at 35 °C on the ZnO, ZnO/CBC_2, and ZnO/CTO_2 materials, and the weight increase is presented in Figure S17. ZnO has no selectivity for CO_2 over N_2, whereas the ZnO/CTO_2 sample shows the highest CO_2 adsorption capacity, with 1.86% of weight increase, which is double the quantity measured for the ZnO/CBC_2 sample (0.80%). The CO_2 desorption process is studied by sweeping the CO_2/N_2 gas mixture for pure N_2 flux followed by the increase of the temperature up to 500 °C (Scheme S1). The developed gases were measured by IR. Figure S18 displays the derivative of the CO_2 desorbed amount for the ZnO/CTO_2 desorption process and the IR spectrum at the maximum gas release. ZnO/CTO_2 shows the maximum release of CO_2 adsorbed molecules at 85 °C and at 440 °C, correlated to the physisorption and chemisorption processes, respectively.[53] The better performance of the ZnO/CTO samples with respect to the ZnO/CBC ones for the CO_2RR under the same conditions could be related to the presence of pyridinic-[52−57] and pyridone-N[39] species in CTO, resulting in more adsorbed CO_2 and facilitating its further reduction in the nearby ZnO-derived active sites.

EIS analysis has been performed at ZnO/CTO_2, ZnO/CBC_2, and ZnO electrodes in order to further elucidate the effect of carbon addition on the ZnO electrical properties. Figure S19 shows the Nyquist plots of the three electrodes at −0.99 V. The experimental curves were analyzed through the circuit depicted in the inset of Figure S19 in order to obtain the resistances related to charge transport (R_t) and charge transfer (R_{ct}).[58] No big difference is observed in the R_{ct} value for the electrodes (see inset of Figure S19). R_t values were found to be not dependent on the potential, in agreement with previous works,[59,60] and equal to 78.96, 30.54, and 14.76 Ω for ZnO, ZnO/CBC_2, and ZnO/CTO_2, respectively. This outcome confirms that the addition of carbon, particularly CTO, can significantly enhance the electrical conductivity of the ZnO-based electrodes, consistent with the widely reported results that biochar can act as electron-transfer mediators and promote direct interspecies electron transfer.[61] Hence, it is

https://doi.org/10.1021/acssuschemeng.1c00837
ACS Sustainable Chem. Eng. 2021, 9, 5445−5453

possible to state that the synergistic effect of CTO could be associated to its high affinity toward the CO_2 reactant due to the pyridinic- and pyridone-N species and the enhanced electron transport due to its high conductivity.[39,52−57] It is also important to notice that the effect of CTO addition on the CO selectivity of ZnO is dependent on the applied potential. As discussed in Figure 3, the CO selectivity of the ZnO electrode is significantly enhanced with the CTO addition at −0.89 V, whereas it is less improved or it even decreases with the CTO addition at −1.09 V. This phenomenon indicates the presence of some negative effects of the CTO carbon besides the aforementioned positive ones in the CO_2RR. As shown in Figure 3, the CTO carbon is demonstrated to have no selectivity for the CO_2RR to CO, and thus its addition could compromise the CO selectivity of ZnO. This negative effect of carbon is more pronounced at higher weight percentages and at more negative potentials as carbon becomes more active for the HER (Figure 3b). Hence, it is of vital importance to optimize the percentage and the type of carbon in order to optimize the performance for the CO_2RR. By comparison, the ZnO/CTO_2 sample shows the optimal selectivity and activity for the CO formation at both applied potentials, highlighting the satisfactory composition of this material for the CO_2RR application.

CO_2 Electrolysis in a Semiflow Cell. To further shed light on the ZnO/CTO material, the CO_2RR has been performed in a wider range of potentials from −0.5 to −1.3 V on the optimal ZnO/CTO_2 and the counterpart ZnO electrodes in a semiflow reactor (Scheme S2b). The detailed $i-t$ curves are presented in Figure S20. As shown in Figure 4a,b, both the CO selectivity and CO production rate are enhanced in the semiflow reactor with respect to those obtained in the batch one on both electrodes at each potential. A good CO selectivity (FE_{CO} > 80%) is observed on the ZnO electrode from −1.1 to −1.3 V, and it is obtained in a wider potential range (−0.9 to −1.3 V) on the ZnO/CTO_2 electrode with a FE_{CO} peak of 85.8% at −1.1 V. The effect of CTO addition is dependent on the applied potentials. At higher potentials (≥−1.0 V), the CTO addition significantly enhances the CO selectivity of ZnO, whereas at lower potentials (<−1.0 V), it remarkably increases the CO production rate, maintaining the good CO selectivity of ZnO. This outcome is in good agreement with the results obtained in the batch reactor. The 14 h CO_2 electrolysis was further performed on ZnO/CTO_2 and ZnO electrodes at −1.1 V. As shown in Figure 4c, the ZnO electrode shows a significant decline in CO selectivity from an initial FE_{CO} value of 81% to a final value of 68%, whereas it shows a negligible decrease in the current density. The ZnO/CTO_2 electrode shows a good retention in both CO selectivity and current density (Figure 4d). FE_{CO} maintains a good value of about 80% at the end of the test, and the current density is even enhanced to 58.2 mA cm^{-2}, indicating the good stability of the ZnO/CTO_2 material under very negative potentials.

Comparison with Other Materials. The CO partial current density, mass activity, and FE_{CO} of ZnO and ZnO/CTO_2 in this work are compared with the reported ZnO-based and other representative metal-based CO-selective electrocatalysts in Table S4. The ZnO/CTO_2 sample shows the FE_{CO} (~80%) value much higher than other Zn-based samples reported in the literature, such as ZnO,[48] electrode-deposited ZnO,[18−20,49,62] dendrite ZnO,[62] nanowire-Zn[16] and Zn nanospheres,[63] and other metal electrocatalysts, such as copper-based electrocatalysts[48,62,64] and N-doped iron materials.[65,66] However, some materials such as S- and P-doped Zn,[47,63] N−C-doped Ni,[66] Au needles,[11] Pd nanoparticles,[15] CuO−Sb_2O_3/CB,[67] and Zn/rGO[28] showed FE_{CO} values superior to the one obtained for the ZnO/CTO_2 sample. Nevertheless, the metal loading in most of these reported works is missing, making it difficult to compare the utilization efficiency of the metal in these works with the one in the ZnO/CTO_2 catalyst. Considering the data available, the ZnO/CTO_2 electrode has mass activity and FE_{CO} that outperform most of the reported electrocatalysts, with the exception of Ni−N−C[66] and 3.7 nm Pd NPs[15] materials. However, it should be highlighted that the ZnO/CTO_2 electrocatalyst was prepared taking into account the sustainable and the circular economy approach with the aim to valorize residues. In summary, CTO biochar is promising as a carbon matrix and can dramatically improve the utilization efficiency of metal-based catalysts for the CO_2RR application. It can also improve the durability of the catalyst and allow long-term and continuous electrolysis. The good stability of ZnO/CTO electrodes, together with their sustainable and simple production, implies the promising potential of the implementation of these materials in real devices. This can be an indication for developing efficient and scalable electrocatalysts for the industrial production of CO from CO_2 conversion.

CONCLUSIONS

ZnO/biochar materials were successfully prepared with different carbon sources (CTO and CBC) and ZnO contents. Both ZnO and ZnO/biochar materials present a hexagonal wurtzite structure and a 3D flower-like architecture with nanoflakes, showing that the addition and increase of biochar content have no effect on the crystalline structure of pristine ZnO. Additionally, ZnO particles appear to be both deposited and/or linked on the carbon surface in both ZnO/CTO and ZnO/CBC samples, as evidenced by the morphological analysis and the spectroscopic techniques that confirm the presence of ZnO−CTO and ZnO−CBC bonds.

Both CTO and CBC alone show no selectivity for the CO_2RR, whereas all ZnO/CTO and ZnO/CBC samples predominantly produce CO. ZnO/CTO samples outperform the ZnO/CBC relatives under the same conditions, which could be related to the presence of pyridinic- and pyridone-N species in CTO that interact with CO_2 molecules and thus help in their electrocatalytic reduction. Moreover, CTO addition significantly enhances the electrical conductivity of the ZnO materials, contributing to the positive synergistic effect between ZnO and CTO. Particularly, ZnO/CTO_2, with 40.6% of carbon, shows the best performance, with good CO selectivity (>80%), in a wide potential range from −0.9 to −1.3 V and the highest CO current density of 75.6 mA cm^{-2}. The ZnO/CTO_2 electrode is demonstrated to be stable at a very negative potential of −1.1 V and high current densities of 50−60 mA cm^{-2}, implying its potential for practical applications. This work extended the use of biochar materials and opened an avenue in the design of biochar/metal oxide composites for electrocatalytic reactions.

ASSOCIATED CONTENT

Supporting Information

The Supporting Information is available free of charge at https://pubs.acs.org/doi/10.1021/acssuschemeng.1c00837.

https://doi.org/10.1021/acssuschemeng.1c00837
ACS Sustainable Chem. Eng. 2021, 9, 5445−5453

Electrochemical characterization methods; XRD results for the pristine biochar materials; all data of FESEM, FTIR, Raman, TGA, and CO_2 adsorption measurements by operando TGA−IR for all materials; XPS fitting results; *i*−*t* curves for all electrodes at various potentials; comparison of geometric current density at various electrodes; comparison of ZnO mass-normalized partial current density for CO production at various electrodes; and EIS analysis on selected electrodes (PDF)

AUTHOR INFORMATION

Corresponding Authors

Mirtha A. O. Lourenço − *Centre for Sustainable Future Technologies (CSFT), Istituto Italiano di Tecnologia-IIT, Turin 10144, Italy;* orcid.org/0000-0003-0260-3422; Email: Mirtha.Lourenco@iit.it

Juqin Zeng − *Centre for Sustainable Future Technologies (CSFT), Istituto Italiano di Tecnologia-IIT, Turin 10144, Italy;* orcid.org/0000-0001-8885-020X; Phone: +39 011 2257719; Email: Juqin.Zeng@iit.it

Authors

Pravin Jagdale − *Centre for Sustainable Future Technologies (CSFT), Istituto Italiano di Tecnologia-IIT, Turin 10144, Italy*

Micaela Castellino − *Department of Applied Science and Technology (DISAT), Politecnico di Torino, Turin 10129, Italy*

Adriano Sacco − *Centre for Sustainable Future Technologies (CSFT), Istituto Italiano di Tecnologia-IIT, Turin 10144, Italy;* orcid.org/0000-0002-9229-2113

M. Amin Farkhondehfal − *Centre for Sustainable Future Technologies (CSFT), Istituto Italiano di Tecnologia-IIT, Turin 10144, Italy*

Candido F. Pirri − *Centre for Sustainable Future Technologies (CSFT), Istituto Italiano di Tecnologia-IIT, Turin 10144, Italy; Department of Applied Science and Technology (DISAT), Politecnico di Torino, Turin 10129, Italy*

Complete contact information is available at: https://pubs.acs.org/10.1021/acssuschemeng.1c00837

Author Contributions

[§]M.A.O.L. and J.Z. contributed equally to this work and are considered "co-first authors". M.A.O.L., J.Z., and C.F.P. contributed to the conceptualization. M.A.O.L. contributed to the syntheses of the CTO sample and of all hybrid ZnO/carbon materials; M.A.O.L. contributed also to the analyses of XRD, TGA, FTIR−ATR, CO_2 adsorption−desorption by operando TGA−IR, and FESEM and to the data analyses of XRD, TGA, FTIR−ATR, Raman, TGA−IR−CO_2, N_2-adsorption−desorption isotherms, and FESEM for all materials. P.J. contributed to the synthesis of the CBC sample and N_2-adsorption−desorption analyses. M.C. contributed to the XPS investigation and the corresponding data analysis. J.Z. contributed to the CO_2 electrolysis measurements and the corresponding data analysis. M.A.F. contributed to the HPLC analysis. A.S. contributed to the EIS analysis. All authors contributed to the manuscript composition.

Notes

The authors declare no competing financial interest.

ACKNOWLEDGMENTS

Mauro Raimondo, Dr. Massimo Rovere, Dr Mattia Bartoli, and Prof. Alberto Tagliaferro are acknowledged for Raman and FESEM analyses. The authors are thankful to IIT for their financial support.

REFERENCES

(1) Costentin, C.; Robert, M.; Savéant, J.-M. Catalysis of the electrochemical reduction of carbon dioxide. *Chem. Soc. Rev.* **2013**, *42*, 2423−2436.

(2) Appel, A. M.; Bercaw, J. E.; Bocarsly, A. B.; Dobbek, H.; DuBois, D. L.; Dupuis, M.; Ferry, J. G.; Fujita, E.; Hille, R.; Kenis, P. J. A.; Kerfeld, C. A.; Morris, R. H.; Peden, C. H. F.; Portis, A. R.; Ragsdale, S. W.; Rauchfuss, T. B.; Reek, J. N. H.; Seefeldt, L. C.; Thauer, R. K.; Waldrop, G. L. Frontiers, opportunities, and challenges in biochemical and chemical catalysis of CO_2 fixation. *Chem. Rev.* **2013**, *113*, 6621−6658.

(3) Feaster, J. T.; Shi, C.; Cave, E. R.; Hatsukade, T.; Abram, D. N.; Kuhl, K. P.; Hahn, C.; Nørskov, J. K.; Jaramillo, T. F. Understanding selectivity for the electrochemical reduction of carbon dioxide to formic acid and carbon monoxide on metal electrodes. *ACS Catal.* **2017**, *7*, 4822−4827.

(4) Li, C. W.; Ciston, J.; Kanan, M. W. Electroreduction of carbon monoxide to liquid fuel on oxide-derived nanocrystalline copper. *Nature* **2014**, *508*, 504−507.

(5) Nielsen, D. U.; Hu, X.-M.; Daasbjerg, K.; Skrydstrup, T. Chemically and electrochemically catalysed conversion of CO_2 to CO with follow-up utilization to value-added chemicals. *Nat. Catal.* **2018**, *1*, 244−254.

(6) Hernández, S.; Farkhondehfal, M. A.; Sastre, F.; Makkee, M.; Saracco, G.; Russo, N. Syngas production from electrochemical reduction of CO_2: Current status and prospective implementation. *Green Chem.* **2017**, *19*, 2326−2346.

(7) Dry, M. E. The Fischer-Tropsch process: 1950-2000. *Catal. Today* **2002**, *71*, 227−241.

(8) Jones, J. H. The Cativa Process for the Manufacture of Acetic Acid: Iridium catalyst improves productivity in an established industrial process. *Platin. Met. Rev.* **2000**, *44*, 94−105.

(9) Qiao, J.; Liu, Y.; Hong, F.; Zhang, J. A review of catalysts for the electroreduction of carbon dioxide to produce low-carbon fuels. *Chem. Soc. Rev.* **2014**, *43*, 631−675.

(10) Kuhl, K. P.; Cave, E. R.; Abram, D. N.; Jaramillo, T. F. Environmental science new insights into the electrochemical reduction of carbon dioxide on metallic copper surfaces. *Energy Environ. Sci.* **2012**, *5*, 7050−7059.

(11) Liu, M.; Pang, Y.; Zhang, B.; Luna, P.; De Luna, O.; Xu, J.; Zheng, X.; Dinh, C. T.; Fan, F.; Cao, C.; de Arquer, F. P. G.; Safaei, T. S.; Mepham, A.; Klinkova, A.; Kumacheva, E.; Filleter, T.; Sinton, D.; Kelley, S. O.; Sargent, E. H. Enhanced electrocatalytic CO_2 reduction via field-induced reagent concentration. *Nature* **2016**, *537*, 382−386.

(12) Chen, Y.; Li, C. W.; Kanan, M. W. Aqueous CO_2 reduction at very low overpotential on oxide-derived Au nanoparticles. *J. Am. Chem. Soc.* **2012**, *134*, 19969−19972.

(13) Shaughnessy, C. I.; Sconyers, D. J.; Lee, H.-J.; Subramaniam, B.; Blakemore, J. D.; Leonard, K. C. Insights into pressure tunable reaction rates for electrochemical reduction of CO_2 in organic electrolytes. *Green Chem.* **2020**, *22*, 2434−2442.

(14) Kim, C.; Jeon, H. S.; Eom, T.; Jee, M. S.; Kim, H.; Friend, C. M.; Min, B. K.; Hwang, Y. J. Achieving selective and efficient electrocatalytic activity for CO_2 reduction using immobilized silver nanoparticles. *J. Am. Chem. Soc.* **2015**, *137*, 13844−13850.

(15) Gao, D.; Zhou, H.; Wang, J.; Miao, S.; Yang, F.; Wang, G.; Wang, J.; Bao, X. Size-dependent electrocatalytic reduction of CO_2 over Pd nanoparticles. *J. Am. Chem. Soc.* **2015**, *137*, 4288−4291.

(16) Li, Y. H.; Liu, P. F.; Li, C.; Yang, H. G. Sharp-tipped zinc nanowires as an efficient electrocatalyst for carbon dioxide reduction. *Chem. —Eur J.* **2018**, *24*, 15486−15490.

(17) Jeon, H. S.; Sinev, I.; Scholten, F.; Divins, N. J.; Zegkinoglou, I.; Pielsticker, L.; Cuenya, B. R. Operando evolution of the structure and oxidation state of size-controlled Zn nanoparticles during CO_2 electroreduction. *J. Am. Chem. Soc.* **2018**, *140*, 9383−9386.
(18) Nguyen, D. L. T.; Jee, M. S.; Won, D. H.; Jung, H.; Oh, H.-S.; Min, B. K.; Hwang, Y. J. Selective CO2 reduction on zinc electrocatalyst: the effect of zinc oxidation state Induced by pretreatment environment. *ACS Sustain. Chem. Eng.* **2017**, *5*, 11377−11386.
(19) Lu, Y.; Han, B.; Tian, C.; Wu, J.; Geng, D.; Wang, D. Efficient electrocatalytic reduction of CO_2 to CO on an electrodeposited Zn porous network. *Electrochem. Commun.* **2018**, *97*, 87−90.
(20) Rosen, J.; Hutchings, G. S.; Lu, Q.; Forest, R. V.; Moore, A.; Jiao, F. Electrodeposited Zn dendrites with enhanced CO selectivity for electrocatalytic CO_2 reduction. *ACS Catal.* **2015**, *5*, 4586−4591.
(21) Moreno-García, P.; Schlegel, N.; Zanetti, A.; Ceden, A.; Dutta, A.; Rahaman, M.; Broekmann, P. Selective electrochemical reduction of CO_2 to CO on Zn-based foams produced by Cu2+ and template-assisted electrodeposition. *ACS Appl. Mater. Interfaces* **2018**, *10*, 31355−31365.
(22) Keerthiga, G.; Chetty, R. Electrochemical reduction of carbon dioxide on zinc-modified copper electrodes. *J. Electrochem. Soc.* **2017**, *164*, H164−H169.
(23) Xiao, X.; Han, B.; Chen, G.; Wang, L.; Wang, Y. Preparation and electrochemical performances of carbon sphere@ZnO core-shell nanocomposites for supercapacitor applications. *Nat. Publ. Gr.* **2017**, *7*, 40167.
(24) Yadav, M. S.; Singh, N.; Kumar, A. Synthesis and characterization of zinc oxide nanoparticles and activated charcoal based nanocomposite for supercapacitor electrode application. *J. Mater. Sci. Mater. Electron.* **2018**, *29*, 6853−6869.
(25) Osman, H.; Su, Z.; Ma, X.; Liu, S.; Liu, X.; Abduwayit, D. Synthesis of ZnO/C nanocomposites with enhanced visible light photocatalytic activity. *Ceram. Int.* **2016**, *42*, 10237.
(26) Yang, C.; Wang, X.; Ji, Y.; Ma, T.; Zhang, F.; Wang, Y.; Ci, M.; Chen, D.; Jiang, A.; Wang, W. Photocatalytic degradation of methylene blue with ZnO@C nanocomposites: Kinetics , mechanism , and the inhibition effect on monoamine oxidase A and B. *NanoImpact* **2019**, *15*, 100174.
(27) Choi, S.; Kim, C.; Suh, J. M.; Jang, H. W. Reduced graphene oxide-based materials for electrochemical energy conversion reactions. *Carbon Energy* **2019**, *1*, 85−108.
(28) Nguyen, D. L. T.; Lee, C. W.; Na, J.; Kim, M.-C.; Tu, N. D. K.; Lee, S. Y.; Sa, Y. J.; Won, D. H.; Oh, H.-S.; Kim, H.; Min, B. K.; Han, S. S.; Lee, U.; Hwang, Y. J. Mass transport control by surface graphene oxide for selective CO production from electrochemical CO2 reduction. *ACS Catal.* **2020**, *10*, 3222−3231.
(29) Lokhande, A. C.; Qattan, I. A.; Lokhande, C. D.; Patole, S. P. Holey graphene: An emerging versatile material. *J. Mater. Chem. A* **2020**, *8*, 918−977.
(30) Duo, S.; Zhong, R.; Liu, Z.; Wang, J.; Liu, T.; Huang, C.; Wu, H. One−step hydrothermal synthesis of ZnO microflowers and their composition−/hollow nanorod−dependent wettability and photocatalytic property. *J. Phys. Chem. Solids* **2018**, *120*, 20−33.
(31) Jia, P.; Tan, H.; Liu, K.; Gao, W. Synthesis, characterization and photocatalytic property of novel ZnO/bone char composite. *Mater. Res. Bull.* **2018**, *102*, 45−50.
(32) Miao, L.; Shi, B.; Stanislaw, N.; Mu, C.; Qi, K. Facile synthesis of hierarchical ZnO microstructures with enhanced photocatalytic activity. *Mater. Sci.-Pol.* **2017**, *35*, 45−49.
(33) Sun, Y.; Wang, L.; Yu, X.; Chen, K. Facile synthesis of flower-like 3D ZnO superstructures via solution route. *CrystEngComm* **2012**, *14*, 3199−3204.
(34) Alshammari, A. S.; Chi, L.; Chen, X.; Bagabas, A.; Kramer, D.; Alromaeh, A.; Jiang, Z. Visible-light photocatalysis on C-doped ZnO derived from polymer-assisted pyrolysis. *RSC Adv.* **2015**, *5*, 27690−27698.
(35) Hu, C.; Hu, X.; Li, R.; Xing, Y. MOF derived ZnO/C nanocomposite with enhanced adsorption capacity and photocatalytic performance under sunlight. *J. Hazard. Mater.* **2020**, *385*, 121599−121613.
(36) Jagdale, P.; Ziegler, D.; Rovere, M.; Tulliani, J. M.; Tagliaferro, A. Waste coffee ground biochar: A material for humidity sensors. *Sensors* **2019**, *19*, 801.
(37) Lourenço, M. A. O.; Nunes, C.; Gomes, J. R. B.; Pires, J.; Pinto, M. L.; Ferreira, P. Pyrolyzed chitosan-based materials for CO_2/CH_4 separation. *Chem. Eng. J.* **2019**, *362*, 364−374.
(38) Tu, Y.; Chen, S.; Li, X.; Gorbaciova, J.; Gillin, W. P.; Krause, S.; Briscoe, J. Control of oxygen vacancies in ZnO nanorods by annealing and their influence on ZnO/PEDOT:PSS diode behaviour. *J. Mater. Chem. C* **2018**, *6*, 1815−1821.
(39) Fan, X.; Zhang, L.; Zhang, G.; Shu, Z.; Shi, J. Chitosan derived nitrogen-doped microporous carbons for high performance CO_2 capture. *Carbon* **2013**, *61*, 423−430.
(40) Gorgulho, H. F.; Gonçalves, F.; Pereira, M. F. R.; Figueiredo, J. L. Synthesis and characterization of nitrogen-doped carbon xerogels. *Carbon* **2009**, *47*, 2032−2039.
(41) Nahil, M. A.; Williams, P. T. Surface chemistry and porosity of nitrogen-containing activated carbons produced from acrylic textile waste. *Chem. Eng. J.* **2012**, *184*, 228−237.
(42) Wójtowicz, M.; Pels, J. R.; Moulijn, J. A. The fate of nitrogen functionalities in coal during pyrolysis and combustion. *Fuel* **1995**, *74*, 507−516.
(43) Al-Gaashani, R.; Radiman, S.; Daud, A. R.; Tabet, N.; Al-Douri, Y. XPS and optical studies of different morphologies of ZnO nanostructures prepared by microwave methods. *Ceram. Int.* **2013**, *39*, 2283−2292.
(44) Laurenti, M.; Canavese, G.; Stassi, S.; Fontana, M.; Castellino, M.; Pirri, C. F.; Cauda, V. A porous nanobranched structure: An effective way to improve piezoelectricity in sputtered ZnO thin films. *RSC Adv.* **2016**, *6*, 76996−77004.
(45) Winiarski, J.; Tylus, W.; Winiarska, K.; Szczygieł, I.; Szczygieł, B. XPS and FT-IR characterization of selected synthetic corrosion Products of zinc expected in neutral environment containing chloride ions. *J. Spectrosc.* **2018**, *2018*, 1−14.
(46) Biesinger, M. C.; Lau, L. W. M.; Gerson, A. R.; Smart, R. S. C. Resolving surface chemical states in XPS analysis of first row transition metals, oxides and hydroxides: Sc, Ti, V, Cu and Zn. *Appl. Surf. Sci.* **2010**, *257*, 887−898.
(47) Luo, W.; Zhang, J.; Li, M.; Züttel, A. Boosting CO production in electrocatalytic CO_2 reduction on highly porous Zn catalysts. *ACS Catal.* **2019**, *9*, 3783−3791.
(48) Zeng, J.; Rino, T.; Bejtka, K.; Castellino, M.; Sacco, A.; Farkhondehfal, M. A.; Chiodoni, A.; Drago, F.; Pirri, C. F. Coupled copper-zinc catalysts for electrochemical reduction of carbon dioxide. *ChemSusChem* **2020**, *13*, 4128−4139.
(49) Qin, B.; Li, Y.; Fu, H.; Wang, H.; Chen, S.; Liu, Z.; Peng, F. Electrochemical reduction of CO2 into tunable syngas production by regulating the crystal facets of earth-abundant Zn catalyst. *ACS Appl. Mater. Interfaces* **2018**, *10*, 20530−20539.
(50) Guo, D.; Shibuya, R.; Akiba, C.; Saji, S.; Kondo, T.; Nakamura, J. Active sites of nitrogen-doped carbon materials for oxygen reduction reaction clarified using model catalysts. *Science* **2016**, *351*, 361−365.
(51) Primo, A.; Forneli, A.; Corma, A.; García, H. From biomass wastes to highly efficient CO_2 adsorbents: graphitisation of chitosan and alginate biopolymers. *ChemSusChem* **2012**, *5*, 2207−2214.
(52) Kiuchi, H.; Shibuya, R.; Kondo, T.; Nakamura, J.; Niwa, H.; Miyawaki, J.; Kawai, M.; Oshima, M.; Harada, Y. Lewis basicity of nitrogen-doped graphite observed by CO_2 chemisorption. *Nanoscale Res. Lett.* **2016**, *11*, 127.
(53) Wu, Q.; Gao, J.; Feng, J.; Liu, Q.; Zhou, Y.; Zhang, S.; Nie, M.; Liu, Y.; Zhao, J.; Liu, F.; Zhong, J.; Kang, Z. A CO_2 adsorption dominated carbon defect-based electrocatalyst for efficient carbon dioxide reduction. *J. Mater. Chem. A* **2020**, *8*, 1205−1211.
(54) Wang, M.; Fan, X.; Zhang, L.; Liu, J.; Wang, B.; Cheng, R.; Li, M.; Tian, J.; Shi, J. Probing the role of O-containing groups in CO_2

https://doi.org/10.1021/acssuschemeng.1c00837
ACS Sustainable Chem. Eng. 2021, 9, 5445−5453

adsorption of N-doped porous activated carbon. *Nanoscale* **2017**, *9*, 17593−17600.
(55) Ren, X.; Li, H.; Chen, J.; Wei, L.; Modak, A.; Yang, H.; Yang, Q. N-doped porous carbons with exceptionally high CO_2 selectivity for CO_2 capture. *Carbon* **2017**, *114*, 473−481.
(56) Saha, D.; Van Bramer, S. E.; Orkoulas, G.; Ho, H.-C.; Chen, J.; Henley, D. K. CO_2 capture in lignin-derived and nitrogen-doped hierarchical porous carbons. *Carbon* **2017**, *121*, 257−266.
(57) Liu, S.; Yang, H.; Huang, X.; Liu, L.; Cai, W.; Gao, J.; Li, X.; Zhang, T.; Huang, Y.; Liu, B. Identifying Active Sites of Nitrogen-Doped Carbon Materials for the CO_2 Reduction Reaction. *Adv. Funct. Mater.* **2018**, *28*, 1800499.
(58) Sacco, A. Electrochemical impedance spectroscopy as a tool to investigate the electroreduction of carbon dioxide: A short review. *J. CO2 Util.* **2018**, *27*, 22−31.
(59) Zeng, J.; Bejtka, K.; Di Martino, G.; Sacco, A.; Castellino, M.; Re Fiorentin, M.; Risplendi, F.; Farkhondehfal, M. A.; Hernández, S.; Cicero, G.; Pirri, C. F.; Chiodoni, A. Microwave-assisted synthesis of copper-based electrocatalysts for converting carbon dioxide to tunable syngas. *ChemElectroChem* **2020**, *7*, 229−238.
(60) Zeng, J.; Bejtka, K.; Ju, W.; Castellino, M.; Chiodoni, A.; Sacco, A.; Farkhondehfal, M. A.; Hernández, S.; Rentsch, D.; Battaglia, C.; Pirri, C. F. Advanced Cu-Sn foam for selectively converting CO_2 to CO in aqueous solution. *Appl. Catal., B* **2018**, *236*, 475−482.
(61) Wan, Z.; Sun, Y.; Tsang, D. C. W.; Hou, D.; Cao, X.; Zhang, S.; Gao, B.; Ok, Y. S. Sustainable remediation with an electroactive biochar system: mechanisms and perspectives. *Green Chem.* **2020**, *22*, 2688−2711.
(62) Ren, D.; Ang, B. S.-H.; Yeo, B. S. Tuning the selectivity of carbon dioxide electroreduction toward ethanol on oxide-derived Cu x Zn catalysts. *ACS Catal.* **2016**, *6*, 8239−8247.
(63) Li, C.; Shen, G.; Zhang, R.; Wu, D.; Zou, C.; Ling, T.; Liu, H.; Dong, C.; Du, X.-W. Zn nanosheets coated with a ZnS subnanometer layer for effective and durable CO_2 reduction. *J. Mater. Chem. A* **2019**, *7*, 1418−1423.
(64) He, J.; Dettelbach, K. E.; Huang, A.; Berlinguette, C. P. Brass and bronze as effective CO_2 reduction electrocatalysts. *Angew. Chem. Int. Ed.* **2017**, *56*, 16579−16582.
(65) Zhao, J.; Deng, J.; Han, J.; Imhanria, S.; Chen, K.; Wang, W. Effective tunable syngas generation via CO2 reduction reaction by non-precious Fe-N-C electrocatalyst. *Chem. Eng. J.* **2020**, *389*, 124323−124330.
(66) Möller, T.; Ju, W.; Bagger, A.; Wang, X.; Luo, F.; Ngo Thanh, T.; Varela, A. S.; Rossmeisl, J.; Strasser, P. Efficient CO_2 to CO electrolysis on solid Ni−N−C catalysts at industrial current densities. *Energy Environ. Sci.* **2019**, *12*, 640−647.
(67) Li, Y.; Chu, S.; Shen, H.; Xia, Q.; Robertson, A. W.; Masa, J.; Siddiqui, U.; Sun, Z. Achieving highly selective electrocatalytic CO_2 reduction by tuning CuO-Sb_2O_3 nanocomposites. *ACS Sustain. Chem. Eng.* **2020**, *8*, 4948−4954.

https://doi.org/10.1021/acssuschemeng.1c00837
ACS Sustainable Chem. Eng. 2021, 9, 5445−5453